Appl Nanosci (2015) 5:515–520
DOI 10.1007/s13204-014-0344-z

ORIGINAL ARTICLE

Synthesis, characterization and magnetic properties of hematite (α-Fe_2O_3) nanoparticles on polysaccharide templates and their antibacterial activity

M. Mohamed Rafi · K. Syed Zameer Ahmed · K. Prem Nazeer · D. Siva Kumar · M. Thamilselvan

Received: 31 March 2014 / Accepted: 29 July 2014 / Published online: 10 August 2014

Abstract The present study is to synthesize iron oxide nanoparticles on different polysaccharide templates calcined at controlled temperature, characterizing them for spectroscopic and magnetic studies leading to evaluate their antibacterial property. The synthesized iron oxide nanoparticles were characterized by X-ray diffractometer (XRD), Fourier transform infrared spectroscopy, high resolution scanning electron microscopy (HRSEM), high resolution transmission electron microscopy (HRTEM) and vibrating sample magnetometer. The iron oxide nanoparticles were tested for antibacterial activity against gram-positive and gram-negative bacterial species. The XRD confirms the crystalline nature of iron oxide nanoparticles with the mean crystallite size of 10 nm. The functional groups of the synthesized iron oxide nanoparticles were 547, 543 and 544 cm^{-1} characterizing the Fe–O and the broad bands at 3,398, 3,439 and 3,427 cm^{-1} were attributed to the stretching vibrations of hydroxyl group absorbed by iron oxide nanoparticles. HRTEM analyses revealed that the average particle size of the hematite nanoparticles are about 85, 92 and 77 nm for AF, DF and GF, respectively, which was a coincident with the results obtained from the HRSEM analysis. Magnetic measurement exhibited ferromagnetic behavior of the α-Fe_2O_3 at the room temperature with higher coercivity of $H_C = 2{,}303$, 2,333 and 1,019 Oe for AF, DF and GF, respectively. Antibacterial test showed the inhibition against *Aeromonas hydrophila* and *Escherichia coli* with significant antagonistic activity.

Keywords Iron oxide nanoparticles · Polysaccharides · Ferromagnetism · Antibacterial activity

M. M. Rafi
Department of Physics, C. Abdul Hakeem College, Melvisharam 632509, Tamilnadu, India

K. S. Z. Ahmed
Department of Biochemistry, C. Abdul Hakeem College, Melvisharam 632509, Tamilnadu, India

M. M. Rafi · K. P. Nazeer (✉) · D. Siva Kumar
PG and Research Department of Physics, Islamiah College, Vaniyambadi 635752, Tamilnadu, India
e-mail: mohamedrafi947@gmail.com; nazeerprem13@gmail.com

M. Thamilselvan
Department of Physics, TPGIT, Vellore 632002, Tamilnadu, India

Introduction

Templating is one of the most frequently used methods of synthesizing materials with structural units ranging from nanometers to micrometers. Aqueous gel-like lyotropic liquid crystal with extensive hydrogen bonding and nanoscale hydrophilic compartments can be employed for direct templating of nanoscale features (Braun et al. 2005). The use of biological materials as templates is gaining momentum and biotemplating takes advantage of the structural stability and specificity of biological systems to create novel materials (Sotiropoulou et al. 2008). Synthesis of well-structured, monodisperse nanostructures of iron oxide has tremendous interest. Such nanostructures are extensively used in magnetic materials, as photocatalyst, in sensors, medical applications such as hyperthermia, targeted drug delivery, magnetic resonance imaging, etc. (Zhao et al. 2005). Choosing the right material for synthesis of iron oxide nanoparticles is crucial by varying the processing conditions with various forms of iron oxides such as Fe_3O_4, γ-$Fe_2O_3$and α-Fe_2O_3. Precipitation of the aqueous

Fe^{2+}/Fe^{3+} solution (Laurent et al. 2008) or in situ generated Fe^{3+} solution results in Fe_3O_4 and γ-Fe_2O_3, while high temperature reaction results in α- Fe_2O_3 (Zhou et al. 2008). Ferromagnetic particles can also be synthesized through the hematite route owing to the higher stability of hematite and then subsequently reduced to magnetite (Zhao et al. 2008). Recently, the use of iron oxide nanoparticles in photonic applications has also been reported (Ge et al. 2008). Agarose is a hydrophilic polymer and is widely used in biomedical applications and bioengineering (Rochas and Lahaye 1989). The basic disaccharide repeating units of agarose consists of (1,3) linked β-D-galactose (G) and (1,4) linked α-L-(3,6)-anhydrogalactose. Dextran is a water-soluble polysaccharide mainly composed of α-D-(1→6) linked glucose units and some α-D-(1→3) linked to glucose branch units. In strongly alkaline solution, dextran interacts with hydroxyl groups present in the iron oxide particles. Gelatin is derived from collagen, and it is commonly used to immobilize drugs and genes to produce controlled released products for pharmaceutical and medical applications (Gupta and Gupta 2008). Gelatin, being water soluble, biodegradable and biocompatible, can also be a promising candidate for the surface modification of iron oxide.

In this communication, we report a simple thermal decomposition route to synthesize α-Fe_2O_3 nanoparticles using only ferrous sulfate hydrate ($FeSO_4 \cdot 7H_2O$) as raw material. The iron oxide bound agarose, dextran and gelatin templates can be used directly by removal of unbound ions, owing to their remarkable stability, biocompatibility and biodegradability. The iron oxide nanoparticles thus synthesized have been characterized for the morphology and magnetic properties. Further, the in vitro antibacterial activities were evaluated against six bacteria including three Gram-positive *Staphylococcus aureus* (*S. aureus*), *Aeromonas hydrophila* (*A. hydrophila*), *Streptococcus pyogenes* (*S. pyogenes*) and three Gram-negative *Pseudomonas aeruginosa* (*P. aeruginosa*), *Enterococcus faecalis* (*E. faecalis*), *Escherichia coli* (*E. coli*) bacteria. To the best of our knowledge, the synergistic impact of magnetic nanoparticles of iron oxide as antibacterial agent is not yet reported so far in the earlier literatures and hence this study is conducted to find the antibacterial activity of magnetic nanoparticles.

Experimental

Materials

All chemicals were procured from M/s Fishur Scientific, India and used without any further purification. Ferrous sulfate ($FeSO_4 \cdot 7H_2O$) was used as source for iron(II) and agarose, dextran and gelatin were the template components of the polysaccharide. High alumina crucibles were employed for the calcination reactions. *Aeromonas hydrophila* (MTCC-1739), *E. coli* (MTCC-1677), *S. aureus* (MTCC-3160), *P. aeruginosa* (MTCC-4030), *E. faecalis* (MTCC-3159) and *S. pyogenes* (MTCC-1928) were obtained from the Institute of Microbial Technology (IMTECH), Chandigarh, India. The lyophilized culture sample was resuspended in nutrient broth with 1.0 % NaCl at 37 °C for 24 h into the viable culture source. All these strains were grown in Tryptic soy broth (TSB) except for *E. coli* strains. *Escherichia coli* strains were grown in Luria–Bertani (LB) medium. The strains were grown aerobically at 37 °C, with 10 mL of medium in 18–150 mm borosilicate glass culture tubes with shaking at 200 rpm under normal laboratory lighting conditions unless specified.

Preparation of agarose-Fe_2O_3 (AF), dextran-Fe_2O_3 (DF), gelatin-Fe_2O_3 (GF)

A quantity of 2.5 g of polysaccharide (agarose, dextran and gelatin) was added to 100 mL distilled water, then the mixture was heated at 90 °C for about 10 min with constant stirring for dissolution of the polysaccharide. 10 g of ferrous sulfate hydrate ($FeSO_4 \cdot 7H_2O$) was added to the solution, the resultant solution was stirred for 30 min. The template–iron mixed solution was treated at 800 °C (heating rate of 5 °C/min) and maintained at that temperature for 120 min, after which it was cooled to room temperature at a rate of 10 °C/min. The so-obtained powder was collected, washed four times in deionized water and ethanol, and dried at 80 °C for 5 h. Thus the obtained sample was characterized.

Characterization techniques

The X-ray diffractometer (Bruker Model: D8 Advance) employing Cu Kα ($\lambda = 1.5406$ Å, $2\theta = 10°$–$80°$) radiation was used to characterize the crystal structure of the sample. IR spectra were recorded with an FTIR spectrometer (Perkin Elmer IR Spectrometer) in the range of 400–4,000 cm^{-1} on pressed disks using KBr as binding material. The surface morphology of the samples was studied by high resolution scanning electron microscopy (HRSEM) (F E I Quanta FEG 200) and high resolution transmission electron microscopy (HRTEM) (JEOL JEM 2100). The magnetic properties of the samples were investigated by using vibrating sample magnetometer (EC&G Princeton Applied Research VSM MODEL 155).

Results and discussion

FTIR spectroscopic studies

The FTIR spectra of agarose, AF, dextran, DF, gelatin and GF are shown in Fig. 1. The dominant bands of the three

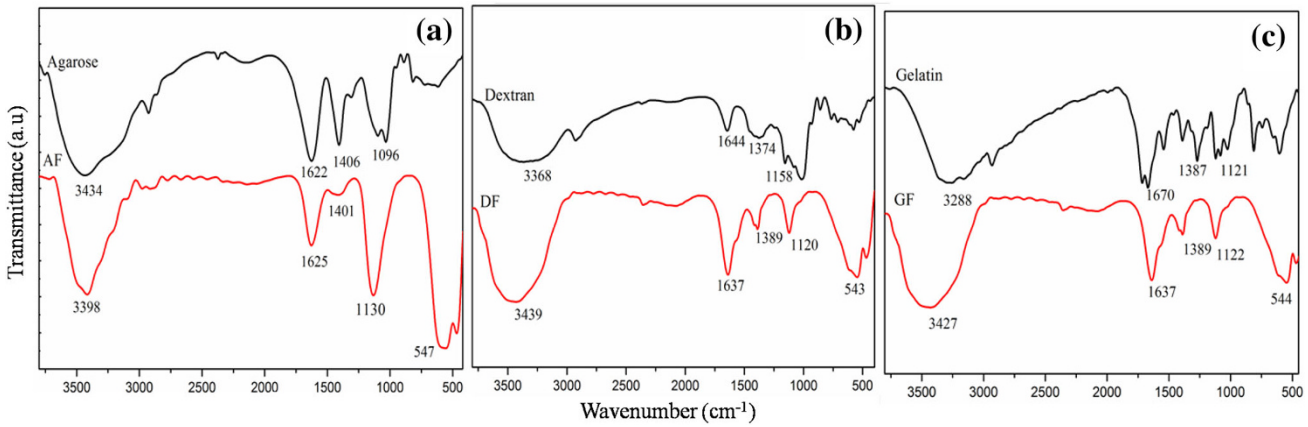

Fig. 1 FTIR spectra of **a** agarose, AF, **b** dextran, DF **c** gelatin, GF

products namely AF at 547 cm^{-1}, DF at 543 cm^{-1} and GF at 544 cm^{-1} are the characteristics of α-Fe_2O_3 (Barron and Torrent 1996). The presence of C–O bond stretching of the C–O–C group in the anhydroglucose ring was observed at 1,096, 1,120 and 1,121 cm^{-1}, respectively (Ma et al. 2009). The bands at 1,406, 1,374 and 1,387 cm^{-1} are due to C–O bond stretching of the C–O–H group. The symmetric stretching vibration of C–O–C groups and bending vibration of water molecules are observed for agarose, dextran and gelatin at 1,622, 1,644 and 1,670 cm^{-1}, respectively (Kormann et al. 1989). The peaks exhibited at 3,398, 3,439 and 3,427 cm^{-1} are attributed to the stretching vibrations of OH, which is assigned to OH-absorbed by iron oxide nanoparticles.

X-Ray diffraction analyses

The powder XRD patterns of AF, DF and GF are shown in Fig. 2. All samples could be indexed to the hexagonal α-Fe_2O_3 phase (JCPDS 33-0664), with no characteristic peaks of other impurities, thus suggesting the high phase purity of the as-synthesized products. The strong and sharp diffraction peaks indicate the high crystallinity of these samples (Liu et al. 2005). The XRD data also revealed that the α-Fe_2O_3 obtained had rhombohedral structure. A hematite crystal has a rhombohedrally centered hexagonal structure of corundum type with a close packed lattice in which two-third of the octahedral sites are occupied by Fe^{3+} ions (Sreeram et al. 2009). In a typical crystal unit, each Fe atom is surrounded by six oxygen atom, where each oxygen atom is bound to four Fe atoms. Due to these characteristics of the corundum structure, the surface hydroxyl configuration of the various crystal face of hematite is quite different (Jitianu et al. 2002). The major diffractions were observed from (012), (104), (110), (024) and (116) planes of α-Fe_2O_3 for all the cases. The average crystallite sizes of the prepared α- Fe_2O_3 were calculated

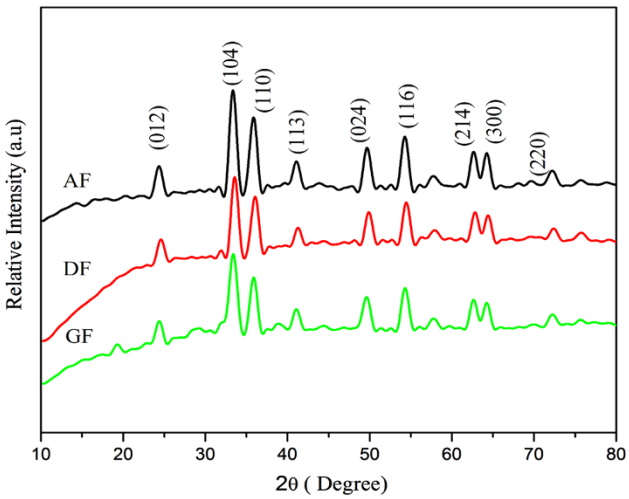

Fig. 2 Powder X-ray diffraction pattern of AF, DF and GF

using Debye–Scherrer equation ($D = 0.9\lambda/(\beta \ \mathrm{Cos}\theta)$), (where, D is the crystallite size (diameter), λ is the wave length of X-ray, i.e., 1.540598 Å, β is the value of FWHM, which is expressed in radians and θ is the Bragg's angle) and found to be around 10 nm.

Morphological studies

The surface morphologies of the prepared AF, DF and GF were studied using high resolution scanning electron microscope, as shown in Fig. 3. It is evident from the HRSEM images that the particles are dumbbell nature and the average size of iron oxide particles are about 90, 97 and 80 nm for AF, DF and GF, respectively. The difference in the crystallite size calculated using X-ray diffraction and particle size obtained by SEM is due to the fact that the particles composed of several crystallization domains are observed by X-rays while whole particle is observed with SEM (Vazquez et al. 1998). The increase in grain size

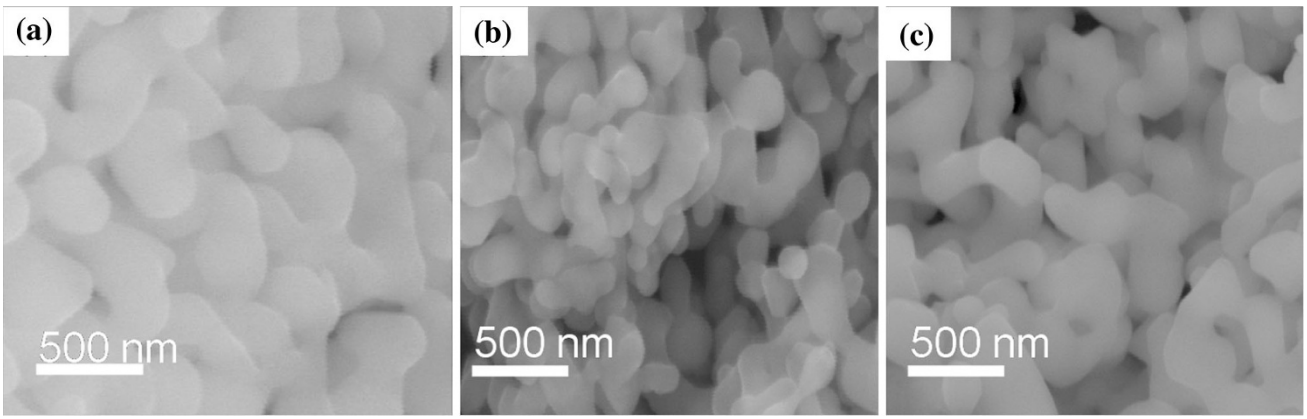

Fig. 3 HRSEM micrographs for **a** AF, **b** DF and **c** GF

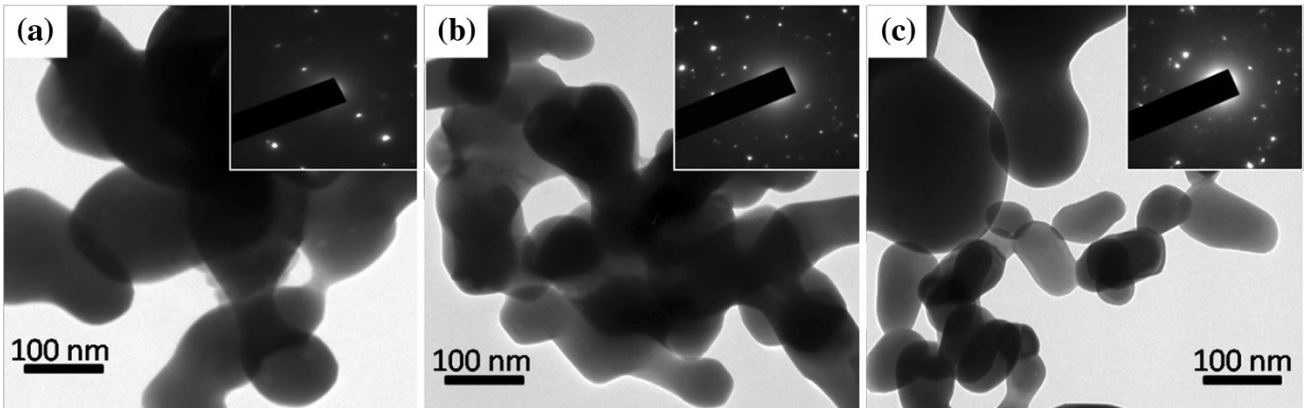

Fig. 4 HRTEM micrographs of **a** AF, **b** DF, **c** GF (*inset* shows SAED patterns)

occurred due to the further agglomeration of primary particles, when the sample was annealed at higher temperature (800 °C).

Further analyses on the hematite nanoparticles are carried out by selected area electron diffraction (SAED) and high resolution TEM (HRTEM). Figure 4a, b, c displays the high magnification TEM image of an AF, DF and GF. The morphology of the nano-sized hematite particles showed a dumbbell shape nature. These dumbbell-shaped nanoparticles are joined together to form bundles of aggregates. The mean size of particles was about 85, 92 and 77 nm for AF, DF and GF which was coincident with the results obtained from the HRSEM analysis. The corresponding selected area electron diffraction (SAED) pattern is shown in inset of Fig. 4. The ED pattern consists of concentric rings along with spots over the rings. This feature indicates the polycrystallinity of the sample (Pawaskar et al. 2002).

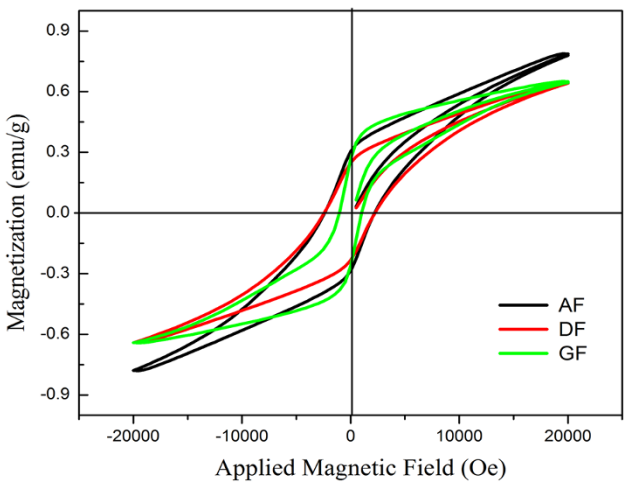

Fig. 5 Magnetization curves of AF, DF and GF at 300 K

Magnetic studies

Generally, the magnetic properties of materials have been dependent on factors, such as the morphology and crystal structure (including impurities or substitutions) of the samples (Cudennec and Lecerf 2006; Subarna et al. 2007). As the size of the hematite particle decreases to the micro/nanometer scale, materials can exhibit unusual magnetic

Table 1 Antibacterial activity of iron oxide nanoparticles

Samples	Gram positive									Gram negative								
	S. aureus (mg/mL)			*A. hydrophila* (mg/mL)			*S. pyogenes* (mg/mL)			*P. aeruginosa* (mg/mL)			*E. faecalis* (mg/mL)			*E. coli* (mg/mL)		
	12.5	25	50	12.5	25	50	12.5	25	50	12.5	25	50	12.5	25	50	12.5	25	50
AF	–	–	+	–	–	++	–	–	+	–	–	+	–	–	–	–	–	++
DF	–	+	++	–	+	+++	–	+	++	–	+	++	–	–	–	–	+	+++
GF	–	–	++	–	+	++	–	–	++	–	–	++	–	–	–	–	+	++

"–" No significant change (or) inhibition

"+" 1 % increase in primary inhibition

"++" 2 % increase in primary inhibition

"+++" 3 % increase in primary inhibition

behaviors that are quite different from those of conventional bulk materials (Sorescu et al. 1999). Figure 5 shows the magnetic hysteresis loops of AF, DF and GF at 300 K in the applied magnetic field sweeping from −20 to 20 kOe. It can be seen that no saturation of the magnetization for all the three samples as a function of the field is observed up to the maximum applied magnetic field, which is similar to the reported literature (Liu et al. 2005; Niederberger et al. 2002). The hysteresis loop indicates that these hematite nanoparticles have ferromagnetic behavior, and the magnetization at the maximum applied magnetic field (M_{max}) are 0.804, 0.650 and 0.640 emu/g for samples AF, DF and GF, respectively. All the three samples possess wide open M-H loops with the remanent magnetization (M_r), the coercivity (H_c) of 0.306, 0.269, 0.267 emu/g, 2,340, 2,333 and 1,019 Oe, respectively. It is clearly seen that the GF exhibited an extremely small hysteresis loop and low coercivity compared to both AF and DF. In the case of AF and DF, both exhibited larger hysteresis loops and coercivity, further confirming that the hematite particle size of GF was smaller than those of AF and DF (Liu et al. 2008). This was also consistent with the findings from HRSEM and HRTEM. The high coercive values may be partly attributed to a surfactant-free surface because no surfactant is used in this study (Cao et al. 2006; Zeng et al. 2008).

Antimicrobial activity

Antibacterial activity of iron oxide nanoparticles was analyzed using well diffusion method against selected bacterial species. Bacterial inoculums were prepared by growing a single colony overnight in nutrient broth and adjusting the turbidity to 0.5 McFarland standards. Mueller–Hinton agar (MHA) plates were inoculated with this bacterial suspension and various volumes of iron oxide nanoparticles in 12.5, 25 and 50 mg/mL were added at the center well with a diameter of 8 mm. These plates were incubated at 37 °C for 24 h. The tetracyclin was used as a positive control for bacterial species as commercial control for the antibacterial assay. The antibacterial agents were used in their commercial presentation to prepare a stock solution adjusted to the concentration of 1.25 mg/mL^{-1} (30 µg per well) (Magaldi et al. 2004). All experiments were done in triplicates to obtain concurrent results and the standard deviations were tabulated (Table 1). The results showed a inhibition on *A. Hydrophila* and *E. coli* with iron oxide nanoparticles. Based upon the antibacterial parameters, the iron oxide nanoparticles did not show any significant changes in dose of 12.5 mg/mL, but there was a considerable increase in the inhibition with the increase in dosage. Similar phenomenon was reported for the antibacterial effect of iron oxide nanoparticles (Tran et al. 2010).

Conclusion

The Iron oxide nanoparticles were synthesized on to novel biopolymer template using the simple thermal decomposition method. As evidenced from FTIR, good interaction between hematite and polysaccharide functional groups controls the hematite crystal growth. The XRD measurements revealed a pure phase α-Fe_2O_3. HRSEM and HRTEM confirmed dumbbell nature of the iron oxide nanoparticles obtained at 800 °C and the lowest particle size was found to be 77 nm for GF. The magnetization measurements of the iron oxide nanoparticles prepared at 800 °C exhibit ferromagnetic behavior at room temperature for all the samples. The hematite nanoparticles have outstanding antimicrobial efficiency against some bacterial pathogens. It is concluded that further exploration on this field is needed to develop eco-friendly bionanomaterials for biomedicines.

References

Barron V, Torrent J (1996) Surface hydroxyl configuration of various crystal faces of hematite and goethite. J Colloid Interf Sci 177:407–410

Braun PV, Osenar P, Twardowski M, Tew GN, Stupp SI (2005) Macroscopic nanotemplating of semiconductor films with hydrogen-bonded lyotropic liquid crystals. Adv Funct Mater 15:1745–1750

Cao H, Wang G, Zhang L, Zhang YS, Zhang X (2006) Shape and magnetic properties of single-crystalline hematite (α-Fe_2O_3) nanocrystals. Chem Phys Chem 7:1897–1901

Cudennec Y, Lecerf A (2006) The transformation of ferrihydrite into goethite or hematite, revisited. J Solid State Chem 179:716–722

Ge J, Yin Y (2008) Magnetically responsive colloidal photonic crystals. J Mater Chem 18:5041–5045

Gupta AK, Gupta M (2008) Synthesis and surface engineering of iron oxide nanoparticles for biomedical applications. Biomaterials 26:3995–4021

Jitianu A, Crisan M, Meghea A, Rau I, Zaharescu M (2002) Influence of the silica based matrix on the formation of iron oxide nanoparticles in the Fe_2O_3–SiO_2 system, obtained by sol–gel method. J Mater Chem 12:1401–1407

Kormann C, Bahnemann DW, Hoffmann MR (1989) Environmental photochemistry: is iron oxide (hematite) an active photocatalyst? A comparative study: α-Fe_2O_3, ZnO, TiO_2. J Photo chem Photo biol A Chem 48:161–169

Laurent S, Forge D, Port M, Roch A, Robic C, Elst LV, Muller RN (2008) Magnetic iron oxide nanoparticles: synthesis, stabilization, vectorization, physicochemical characterizations, and biological applications. Chem Rev 108:2064–2110

Liu XM, Fu SY, Xiao HM, Huang CJ (2005) Preparation and characterization of shuttle-like α Fe_2O_3 nanoparticles by supermolecular template. J Solid State Chem 178:2798–2803

Liu SL, Zhang LN, Zhou JP, Xiang JF, Sun JT, Guan JG (2008) Fiber like Fe_2O_3 macroporous nanomaterials fabricated by calcinating regenerate cellulose composite fibers. Chem Mater 20:3623–3628

Ma XF, Chang PR, Yang JW, Yu JG (2009) Preparation and properties of glycerol plasticized-pea starch/zinc oxide-starch bionanocomposites. Carbohydr Polym 75:472–478

Magaldi S, Mata-Essayag S, Hartung de Capriles C, Perez C, Colella MT, Olaizola C, Ontiveros Y (2004) Well diffusion for antifungal susceptibility testing. Int J Infect Dis 8:39–45

Niederberger M, Krumeich F, Hegetschweiler K, Nesper R (2002) An iron polyolate complex as a precursor for the controlled synthesis of monodispersed iron oxide colloids. Chem Mater 14:78–82

Pawaskar NR, Sathaye SD, Bhadbhade MM, Patil KR (2002) Applicability of liquid–liquid interface reaction technique for the preparation of zinc sulfide nano particulate thin films. Mater Res Bull 37:1539–1545

Rochas C, Lahaye M (1989) Average molecular-weight and molecular-weight distribution of agarose and agarose-type polysaccharides. Carbohydr Polym 10:289–298

Sorescu M, Brand RA, Tarabasanu DM, Diamandescu L (1999) The crucial role of particle morphology in the magnetic properties of haematite. J Appl Phys 85:5546–5548

Sotiropoulou S, Sierrasastre Y, Mark SS, Batt CA (2008) Biotemplated nanostructured materials. Chem Mater 20:821–834

Sreeram KJ, Nidhin M, Nair BU (2009) Synthesis of aligned hematite nanoparticles on chitosan–alginate film. Colloids Surf B 71:260–267

Subarna M, Soumen D, Kalyan M, Subhadra C (2007) Synthesis of a α-Fe_2O_3 nanocrystal in its different morphological attributes: growth mechanism, optical and magnetic properties. Nanotechnology 18:275608

Tran N, Mir A, Mallik D, Sinha A, Nayar S, Webster TJ (2010) Bactericidal effect of iron oxide nanoparticles on *Staphylococcus aureus*. Int J Nano med 5:277–283

Vazquez CV, Blanco MC, Quintela MA, Sanchez RD, Rivas J, Oseroff SB (1998) Characterization of $La_{0.67}Ca_{0.33}MnO_{3\pm\delta}$ particles prepared by the sol–gel route. J Mater Chem 8:991–1000

Zeng SY, Tang KB, Li TW, Liang ZH, Wang D, Wang YK, Qi YX, Zhou WW (2008) Facile route for the fabrication of porous hematite nanoflowers: its synthesis, growth mechanism, application in the lithium ion battery, and magnetic and photocatalytic properties. J Phys Chem C 112:4836–4843

Zhao W, Gu J, Zhang L, Chen H, Shi J (2005) Fabrication of uniform magnetic nanocomposite spheres with a magnetic core/mesoporous silica shell structure. J Am Chem Soc 127:8916–8917

Zhao W, Chen H, Li Y, Li L, Lang M, Shi J (2008) Uniform rattle-type hollow magnetic mesoporous spheres as drug delivery carriers and their sustained-release property. Adv Funct Mater 18:2780–2788

Zhou H, Wong SS (2008) A facile and mild synthesis of 1-D ZnO, CuO and α-Fe_2O_3 nanostructures and nanostructured arrays. ACS Nano 2:944–958